

## A Simplified Ice–Ocean Coupled Model for the Antarctic Ice Melt Season

KAY I. OHSHIMA

*Institute of Low Temperature Science, Hokkaido University, Sapporo, Japan*

SOHEY NIHASHI

*Laboratory for Hydrospheric Processes, NASA Goddard Space Flight Center, Greenbelt, Maryland*

(Manuscript received 19 November 2003, in final form 17 May 2004)

### ABSTRACT

In the Antarctic Ocean, sea ice melts mostly by warming of the ocean mixed layer through heat input (mainly solar radiation) in open water areas. A simplified ice–upper ocean coupled model is proposed in which sea ice melts only by the ocean heat supplied from the air. The model shows that the relationship between ice concentration (i.e., fraction,  $C$ ) and mixed layer temperature ( $T$ ) converges asymptotically with time ( $C$ – $T$  relationship), which agrees with observed  $C$ – $T$  plots during summer in the sector 25°–45°E. This relationship can be used for estimating the bulk heat transfer coefficient between ice and ocean by fitting to observations, and a value of  $1.2 \times 10^{-4} \text{ m s}^{-1}$  is obtained. The model shows that the ratio of the heat used for melting to the heat input through open water is inclined to be determined as a function of ice concentration. For typical conditions in the Antarctic ice melt season, the ratio ranges mostly between 0.7 and 0.9. When the model is extended to two dimensions in the meridional direction, with the inclusion of wind forcing, it approximately reproduces the meridional retreat of the Antarctic sea ice. This two-dimensional model can describe the open water–albedo feedback effect, which partly explains the year-to-year variation of the sea-ice retreat in the Antarctic Ocean.

### 1. Introduction

In seasonal and marginal ice zones, heat input through the open water area from the atmosphere is a very important heat source for the sea ice melting (Maykut and Perovich 1987). In the Antarctic Ocean, having a relatively large fraction of open water because of the divergent drift of ice, this heat input is particularly important for sea ice decay. Further, from a calculated net heat flux, surface melting appears to be small, unlike the Arctic case (Andreas and Ackley 1982). Net heat flux over open water during the active melt season reaches 100–150  $\text{W m}^{-2}$  because of large solar heating, and the total heat of this flux is comparable to the latent heat of sea ice melt in the whole Antarctic sea ice zone (Nihashi and Ohshima 2001a). During the active melt season, this heat is much larger than the estimated heat entrained from the deeper ocean, another possible heat source. Therefore, in the summer Antarctic Ocean, heat input through open water area from the atmosphere is the main heat source for sea ice melt.

This heat balance is also suggested from in situ observations. Ohshima et al. (1998) found that in the Antarctic ice melt season the ice concentration is negatively correlated with the upper-ocean temperature and positively correlated with the salinity for the spatially averaged data. This relationship can be explained by assuming that sea ice melt is mostly caused by heat supplied to the upper ocean from the atmosphere. This also suggests that the upper ocean and sea ice are strongly coupled thermodynamically in the ice melt season.

If sea ice is primarily melted by heat input through open water, the following positive feedback is possible in the ice–upper ocean coupled system: once the ice concentration is decreased, the heat input to the upper ocean is enhanced because of larger absorption of solar radiation in the increased open water area, leading to a further decrease in ice concentration through the sea ice melt by the oceanic heat. This effect is regarded as the open water–albedo feedback. Ackley et al. (2001) applied this feedback mechanism to the Ronne polynya during the 1997/98 summer season; the anomalously large open water area was initiated by an anomalous divergent wind field. They summarized that the open water area was enhanced by melting through this feedback mechanism. A numerical model supported this idea (Hunke and Ackley 2001) by a sensitivity study with and without the open water–albedo feedback.

---

*Corresponding author address:* Kay I. Ohshima, Institute of Low Temperature Science, Hokkaido University, Kita-19, Nishi-8, Kitaku, Sapporo 060-0819, Japan.  
E-mail: ohshima@lowtem.hokudai.ac.jp

Some of the large-scale ice–ocean coupled models have incorporated bottom and lateral ice melt by heat input through open water areas, as well as surface melting. In these models, the seasonal cycle of sea ice can be roughly reproduced even in a model that excludes dynamical processes, suggesting to a first approximation that the local thermal balance determines the sea ice retreat in the Antarctic Ocean (e.g., Parkinson and Washington 1979). According to the coupled model of Fichefet and Maqueda (1997), Antarctic sea ice decay is considerably suppressed when solar radiation input in the upper ocean is removed. This suggests that the heat supplied to the upper ocean from the atmosphere and subsequent lateral and bottom melting of sea ice are the main factors in sea ice decay. Ogura et al. (2004) also derived a similar conclusion from their ice–ocean–atmosphere coupled model.

To date, there have been several ice–ocean fully coupled models developed for the Antarctic Ocean (Hibler and Ackley 1983; Stössel et al. 1990, 1998; Häkkinen 1995; Wu et al. 1997; Bailey and Lynch 2000; Timmermann et al. 2002; Fichefet et al. 2003), some of which were successful in reproducing the interannual variations of sea ice. Through these developments of sophisticated coupled models, the simulation of the behavior of Antarctic sea ice has been greatly improved. However, the cause of its interannual variations has not yet been understood well. Another model approach is to extract the essence of the observed features with a model formulated as simply as possible. For example, Roed (1984) examined the thermodynamic coupled ice–ocean system with a simplified model suitable for the marginal ice zone. This paper also takes a simplified model approach focusing on the Antarctic ice melt season.

The primary purpose of this study is to propose a simple ice–upper ocean coupled model that can describe the main observed features in the Antarctic melt season and then to examine the nature of that system. The key assumption is that the heat input through open water is the only heat source for ice melt. This greatly minimizes the complexity of the coupled system. The second purpose is to describe the open water (ice)–albedo feedback using this simplified model, with application to year-to-year variation of sea ice retreat in the Antarctic Ocean. Finally, in this model, a key parameter that cannot be directly obtained by observations is the bulk heat transfer coefficient between ice and ocean ( $K_b$ ). We propose an appropriate value of  $K_b$  that explains the observations.

The organization of the paper is as follows. Section 2 presents a simple coupled model, in which averaged ice thickness is assumed to be constant. In section 3, the model is extended to two dimensions in the meridional direction, which can describe the albedo feedback effects. Section 4 presents a more general model in which the assumption of the constant ice thickness is relaxed. Section 5 provides a summary and discussion.

## 2. A model for an ice–upper ocean coupled system

The key assumption that will be used in our model is that the heat input through open water area is the only heat source for the ice melt. Before describing the model in detail, we briefly discuss the validity of this assumption. One other possible heat source is the direct heat input at the ice surface. According to a heat budget analysis (Nihashi and Ohshima 2001a), the net heat input at the ice surface during the Antarctic summer is less than  $10 \text{ W m}^{-2}$  over the whole Antarctic sea ice zone, one or two orders smaller than that at the water surface because of the difference in albedo. This implies that only a small amount of ice is melted from the ice surface. Actually, satellite remote sensing data (Drinkwater and Liu 2000) and in situ observations (Jeffries et al. 1994) showed that surface and internal melt occurs only in limited areas in the Antarctic Ocean—the perennial ice zone or near-coast area.

Another important potential heat source is the entrainment flux from the deeper ocean. Since the summer oceanic surface layer is strongly stratified both by heating and melting, entrainment of heat from the deeper ocean is suppressed. Further, winter water (WW), whose temperature is nearly at the freezing point, exists beneath the surface layer and prevents the underlying warm Circumpolar Deep Water (CDW) from reaching the surface. At least in the Antarctic summer, the heat flux from the deeper ocean is probably at most  $10 \text{ W m}^{-2}$  (Gordon and Huber 1990). Based on a heat budget analysis, Nihashi and Ohshima (2001a) showed that an assumed spatially uniform flux from the deeper ocean of  $10 \text{ W m}^{-2}$  is less than 25% of the total heat input through open water from the atmosphere during the active melting period (December–January). Ignoring the deeper ocean heat flux appears to be valid during the active melt season as a first-order approximation.

Here we propose a simple thermodynamic ice–upper ocean model, schematically shown in Fig. 1. The upper ocean is simply represented by a mixed layer of thickness  $H$  with a uniform temperature  $T$ . The net heat budget over the ice-covered area fraction  $C$  is assumed to be zero; thus the total surface heat flux  $F_n$  is only applied in the open water fraction,  $1 - C$ . Heat and water exchanges with the ocean below the mixed layer are also assumed to be zero. The ice thickness  $h_0$  is defined as the average thickness of individual ice floes composing the ice medium, assumed to be constant in this section.

The heat balance of the upper ocean is given by

$$c_w \rho_w H \frac{dT}{dt} = F_n (1 - C) + L_f \rho_i h_0 \frac{dC}{dt}, \quad (1)$$

where  $c_w$  ( $=3990 \text{ J kg}^{-1} \text{ }^\circ\text{C}^{-1}$ ) is the heat capacity of seawater;  $\rho_w$  ( $=1026 \text{ kg m}^{-3}$ ) and  $\rho_i$  ( $=900 \text{ kg m}^{-3}$ ) are the densities of seawater and sea ice, respectively;  $L_f$  is the latent heat of fusion for sea ice; and  $t$  is time. We

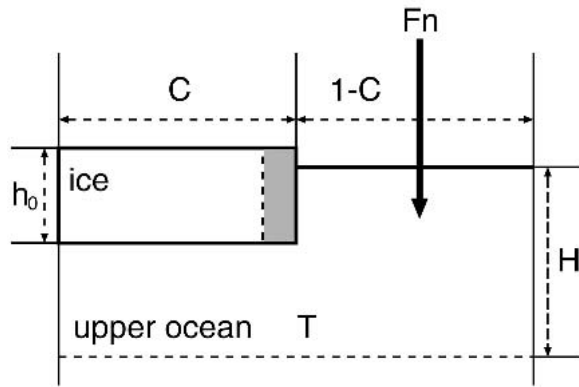


FIG. 1. A schematic illustration of the ice–ocean coupled model:  $C$  is ice concentration (fraction), and thus  $1 - C$  is the open water fraction. In this sketch all the ice is, for convenience, shown as a single piece with average thickness. In reality, the individual ice floes composing the ice medium are randomly distributed within the unit area, interspersed by patches and leads of open water. The average ice thickness is assumed to be constant  $h_0$ , and thus the ice melt is represented only by a decrease in ice concentration. The upper ocean is simply represented by one layer of thickness  $H$  with a uniform temperature  $T$ . Heat flux  $F_n$  is supplied only over the open water area.

use a fixed value of  $L_f = 0.276 \text{ MJ kg}^{-1}$ , corresponding to an ice salinity of 6 psu.

We assume that sea ice melts at a rate proportional to the difference between the water temperature and the freezing point  $T_f$  ( $= -1.86^\circ\text{C}$ ). We implicitly assume that the open water is well mixed with the water just under the ice bottom. Then the melting rate of sea ice,  $-L_f \rho_i h_0 (dC/dt)$ , is parameterized as

$$-L_f \rho_i h_0 \frac{dC}{dt} = c_w \rho_w K_b C (T - T_f), \quad (2)$$

where  $K_b$  is the bulk heat transfer coefficient between ice and ocean. This formulation is basically similar to that of McPhee (1992), Steele (1992), and some recent models (Hunke and Ackley 2001; Timmermann et al. 2002), where  $K_b$  in our study corresponds to  $c_h \times u_\tau$  ( $c_h$ : heat transfer coefficient;  $u_\tau$ : friction velocity) in their studies.

Sea ice ablates through bottom and lateral melting of each ice floe or through breaking into smaller pieces and subsequent melting of brash ice. The present model does not treat the melting of individual ice floes. The model considers this process in a bulk fashion and the melting is represented only by an overall areal change of sea ice since even bottom melting indirectly contributes to the areal change through making very thin ice that finally melts away.

When considering a model in a bulk way, the spatial scale of the model is an important factor because the parameterization and the associated bulk coefficient depend on that spatial scale. Here we consider a scale at which the local balance is satisfied in an area-averaged

sense and the ice and ocean can sufficiently interact. The latter condition arises from (2); the formulation that ice melt is proportional to sea ice concentration implicitly assumes that the ice and ocean can sufficiently interact in that bulk area. We choose 30 km as a typical scale of the model based on the following. Ohshima et al. (1998) found, from the relationship among ice concentration, temperature, and salinity in the upper ocean, that the local balance of heat and salinity approximately holds over a scale of 20–30 km in the Antarctic summer, while at smaller spatial scales, ice advective effects become dominant. Second, the ice migration scale due to the atmosphere synoptic disturbances is  $\sim 30$  km. Over this scale the ice can interact with the upper ocean by drifting on it back and forth. In the ice retreat season, geostrophic wind over the sea ice has an averaged speed of  $\sim 10 \text{ m s}^{-1}$  with a spectral peak at periods of 8–12 days, according to the European Centre for Medium-Range Weather Forecasts reanalysis (ERA-15) data. If we assume a typical wind-forced ice drift of  $1 \text{ cm s}^{-1}$  both from the ice drift at 1% of the geostrophic wind speed and the buoy observations (Kottmeier and Sellmann 1996) with unidirectional forcing for 4 days, the ice migration spatial scale becomes  $\sim 30$  km.

Equations (1) and (2) can be combined and rewritten as

$$H \frac{dT}{dt} = \frac{F_n}{c_w \rho_w} (1 - C) - K_b C (T - T_f). \quad (3)$$

The system of (2) and (3) is one of the simplest models for the Antarctic ice melt season but still represents a system of two nonlinear coupled equations.

Here all parameters are set to values suitable for the region between  $25^\circ$  and  $45^\circ\text{E}$  since the results will be compared with the observations there. The net heat input at the water surface,  $F_n$ , is set to a constant value of  $140 \text{ W m}^{-2}$  (see Fig. 2), based on the calculation with a similar method to that in Nihashi and Ohshima (2001a). In this paper we use the convention that positive fluxes are directed downward. The mixed layer thickness  $H$  is set to 25 m, and the averaged ice thickness is set to 1 m (Ohshima et al. 1998; Worby et al. 1998). The value of  $K_b$  ( $= 1.2 \times 10^{-4} \text{ m s}^{-1}$ ) will be discussed later. The result from these parameter values is defined as the baseline case.

The properties of the solution to (2) and (3) can be discussed in terms of the trajectories in the  $(C, T)$  plane (the phase plane). Figure 3a shows the trajectories of  $T$  as a function of  $C$  in the baseline case for several different initial conditions. With  $C$  decreasing, all trajectories converge asymptotically to a single curve, independent of initial condition. This is an inherent characteristic of the given nonlinear dynamical system. This concentration and temperature relationship is called a  $C$ – $T$  relationship hereinafter. The convergent character arises from a negative feedback, caused by the second term of the right-hand side of (3). If  $T$  is above the

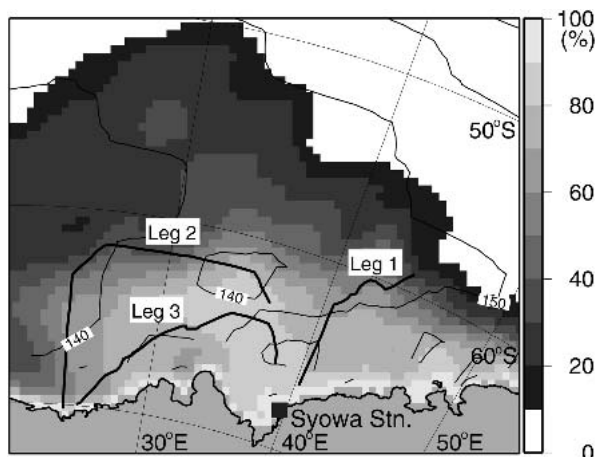


FIG. 2. Sea ice concentration (shown by shading) and the net heat flux at water surface (shown by contours with a contour interval of  $10 \text{ W m}^{-2}$ ) off Syowa Station averaged over Dec 1990, superimposed on the cruise tracks (thick solid lines) of the  $C$ - $T$  plot observations on leg 1 (15–16 Dec), leg 2 (18–20 Dec), and leg 3 (28–30 Dec).

curve, ice melt, proportional to  $T - T_f$ , is enhanced and thereby the latent heat release lowers  $T$ . If  $T$  is below the curve, ice melt is reduced and a continuous flux of  $F_n$  raises  $T$ . A characteristic time scale,  $H/K_b$ , is given in (3). In the present case,  $H/K_b$  is  $\sim 2.4$  days. Figure 3a shows that the trajectories converge at  $\sim 10$  days (triangle and circle dots in Fig. 3a designate 5 and 10 days after the integration, respectively) within the order of this time scale.

The asymptotic curve of convergence is difficult to compute analytically, but it can be obtained by integration with the initial conditions of  $T = T_f$  and  $C \sim 1$ . We briefly show the dependence of the asymptotic curve on the controlling factors, which are  $F_n$ ,  $K_b$ ,  $h_0$ , and  $H$ . It is found that the curve is determined by two parameters  $F_n/K_b$  and  $h_0/H$ . Even for different  $F_n$  or  $h_0$ , the curve is identical for the same  $F_n/K_b$  or  $h_0/H$ . The asymptotic value of  $T$  increases with an increase of  $F_n/K_b$  and  $h_0/H$  (Fig. 3b). The asymptotic curve is more sensitive to the parameter  $F_n/K_b$ .

This  $C$ - $T$  relationship agrees with the observed concentration-temperature ( $C$ - $T$ ) plots by Ohshima et al. (1998). Figure 3c shows the observed  $C$ - $T$  plots from the three legs off Syowa Station ( $25^\circ$ – $45^\circ$ E) in December of 1990, where ice concentration data were collected with a video monitoring system and upper-ocean temperature data were taken at a depth of 8 m in an intake system. We use the 30-km spatial averaged data for both concentration and temperature since the results are compared to the model with typical spatial scale of  $\sim 30$  km. Even though the data were taken in somewhat different ice regimes (see Fig. 2 for cruise tracks of the legs),  $C$ - $T$  plots from the three legs show similar features. In this plot, convergent curves with three values of the bulk heat exchange coefficient  $K_b$ ,

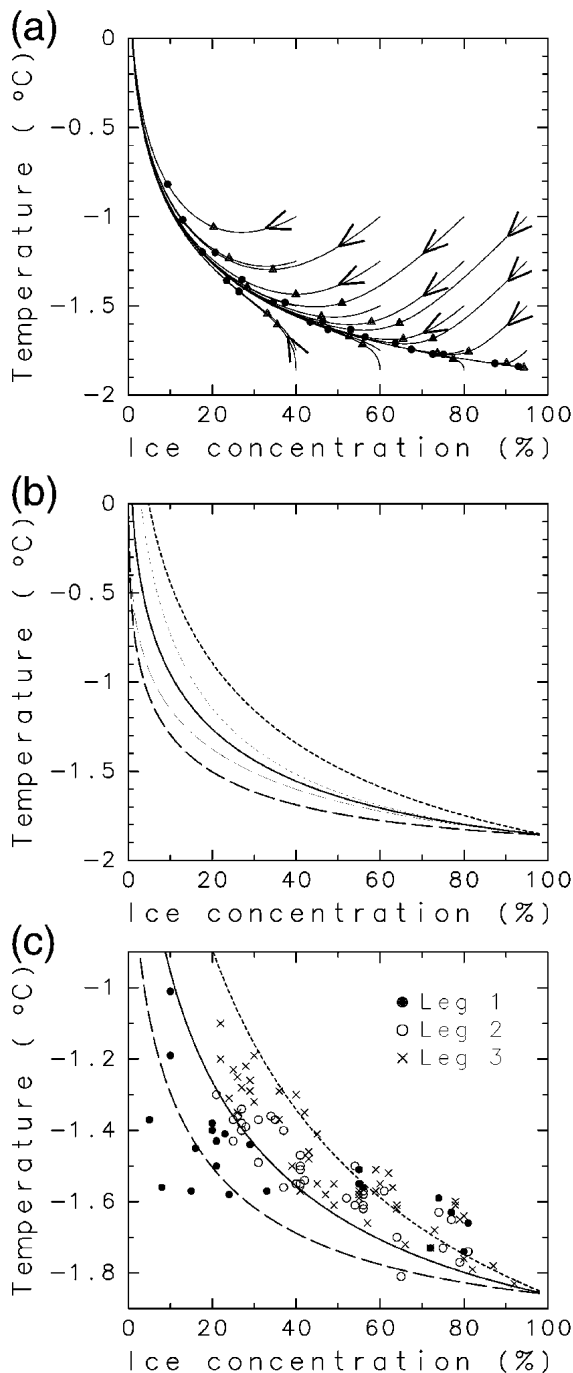


FIG. 3. Relationship between ice concentration and upper-ocean temperature, derived from the ice-ocean coupled model of (2) and (3). (a) Trajectories in the concentration and temperature plane for several different initial conditions. Arrows indicate the direction of time evolution. (b) The convergent (asymptotic) curves with different parameters. Thick solid curve indicates the baseline case. Thick (thin) dashed and dotted curves indicate cases for the half and doubled  $F_n/K_b$  ( $h_0/H$ ) value from the baseline case. (c) The convergent curves with  $K_b = 0.6 \times 10^{-4} \text{ m s}^{-1}$  (dotted curve),  $K_b = 1.2 \times 10^{-4} \text{ m s}^{-1}$  (solid curve), and  $K_b = 2.4 \times 10^{-4} \text{ m s}^{-1}$  (dashed curve), superimposed on observed concentration-temperature plots (30-km spatial averaged data) off Syowa Station in Dec 1990.

(identical to the curves for three values of  $F_n/K_b$  in Fig. 3b) are superimposed. The model curve with  $K_b = 1.2 \times 10^{-4} \text{ m s}^{-1}$  is most consistent with the observed data, through the least squares fitting.

Ohshima et al. (1998) found a similar convergent characteristic in the case in which melting occurs only on the bottom, that is,  $h_0(dC/dt)$  is replaced by  $C(dh/dt)$  in (1) and (2). In this case the system can be solved analytically;  $T$  asymptotically approaches  $T_f + F_n(1 - C)/(c_w\rho_w K_b C)$  with an  $e$ -folding time scale of  $H/(K_b C)$ . However, given that  $C$  is rapidly decreasing in the active melt season, an assumption of constant  $C$  is unrealistic. Thus, the present model seems to be a more applicable one in the Antarctic melt season.

Figure 4a shows the ratio of the heat used for ice melt to the heat input into open water from the air, derived from the coupled system of (2) and (3). Parameter val-

ues and initial conditions are the same as those in Fig. 3a (baseline case). It is found that the heat ratio also converges asymptotically to a single curve with the time scale of  $H/K_b$ , as in the case of  $(C, T)$  plane. This implies that the heat used for ice melt is inclined to be determined by ice concentration for a given heat flux condition. The convergent curve of the heat ratio is determined only by a single parameter  $(F_n H)/(K_b h_0)$ . The asymptotic value of the heat ratio increases with a decrease of  $(F_n H)/(K_b h_0)$  (Fig. 4b). Overall ice concentration in the Antarctic melt season mostly ranges between 0.3 and 0.9. The heat ratios for this parameter range are mostly within 0.7–0.9, implying that heat input through open water is mostly used for sea ice melt but not completely.

### 3. Two-dimensional model for meridional ice retreat

#### a. Model configuration

In the Antarctic Ocean, the sea ice drift, winds, and ocean currents are roughly uniform in the zonal direction. Based on the assumption of uniformity in the zonal direction, the model is extended in two dimensions with the inclusion of ice advection to simulate the meridional retreat of sea ice. The two-dimensional approach for the Antarctic sea ice was first done by Pease (1975).

The upper ocean is modeled in the same manner as described in the previous section. The mixed layer temperature is determined by the local balance of (3), where the net heat input in open water is assumed to be  $F_n(x, t)$ , a function of latitude and time. For ice concentration  $C(x, t)$ , the advection, diffusion, and mechanical redistribution terms are added and thus (2) is modified as follows:

$$\frac{dC}{dt} = -\frac{a_0}{h_0} C(T - T_f) - U(x, t) \frac{\partial C}{\partial x} + A_H \frac{\partial^2 C}{\partial x^2} + \psi_C. \quad (4)$$

Change in ice concentration is determined by the sum of the local ice melt (first term of the right-hand side), net advection of sea ice by wind forcing (second term), horizontal diffusion (third term), and ice resistance (fourth term). The  $x$  coordinate is taken as the meridional direction with northward positive;  $a_0 = (c_w \rho_w K_b)/(\rho_i L_f)$ ; and  $U(x, t)$  is the meridional component of wind-forced ice drift as a function of latitude and time. In this system,  $C(x, 0)$ ,  $F_n(x, t)$ , and  $U(x, t)$  are specified and the time evolution of  $C(x, t)$  and  $T(x, t)$  is calculated. Although the value of  $K_b$  in (3) depends on ocean stratification and wind condition, we used the constant value of  $K_b = 1.2 \times 10^{-4} \text{ m s}^{-1}$ , estimated from the  $C$ - $T$  relationship;  $H$  and  $h_0$  are set to 25 and 1 m, respectively, as in section 2.

Dynamic and thermodynamic change in the sea ice

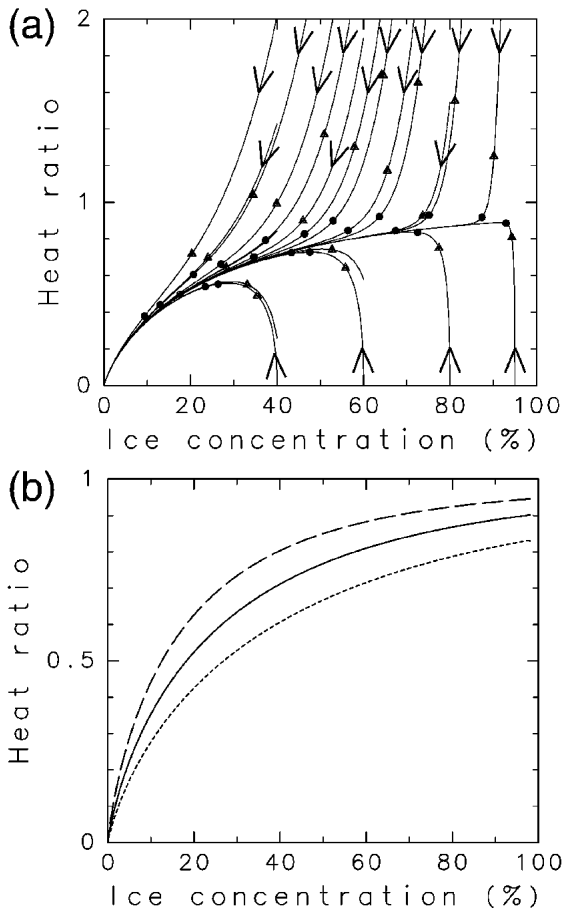


FIG. 4. The ratio of the heat used for ice melt to the heat input through open water as a function of ice concentration, derived from the ice-ocean coupled model (2) and (3). (a) Time evolution for the baseline case with several different initial conditions. The initial conditions and symbols are the same as those of Fig. 3a. (b) The convergent (asymptotic) curves for the baseline case (solid curve), for the case of half  $(F_n H)/(K_b h_0)$  value from the baseline case (dashed curve), and for the case of doubled  $(F_n H)/(K_b h_0)$  value (dotted curve).

field occurs by disturbances with synoptic time scale as well as those with seasonal time scale. The effects of atmospheric synoptic disturbances and mesoscale ocean disturbances are represented by the horizontal diffusion term (third term). Based on a typical ice velocity of  $0.1 \text{ m s}^{-1}$ ,  $u_s$ , and an ice migration scale of  $\sim 30 \text{ km}$ ,  $L_s$ , by synoptic disturbances, the lateral diffusion coefficient,  $A_H$ , should be the order of  $u_s \times L_s$ . Here  $A_H$  is set to  $5.0 \times 10^3 \text{ m}^2 \text{ s}^{-1}$ .

We assume a maximum ice concentration,  $C_{\max}$ , of 95%, based on observations of a relatively large area of leads and open water in the Antarctic Ocean. In the ice convergent zone, specifically in the vicinity of the Antarctic coast, the ice concentration in the model would exceed unity or  $C_{\max}$  without ice resistance. The term  $\psi_C$  in (4) represents ice resistance, which redistributes the ice concentration so as not to exceed  $C_{\max}$ . We treat this resistance in the simplest way, similar to that of Parkinson and Washington (1979). For a grid cell at which the ice concentration,  $C_0$ , exceeds  $C_{\max}$  at a given time step, we reduce the amount of advected ice into this grid cell from the adjacent cells through multiplication by  $(R + C_{\max} - C_0)/R$ , where  $R$  is defined as the increased ice concentration by advection from the adjacent cells at that time step. This method generally requires several iterations. The iterative procedure continues until no grid cell has an ice concentration exceeding  $C_{\max}$ .

#### b. Results for 25°–45°E sector

We choose the sector between 25° and 45°E as a test simulation area. The geographical location of this sector is relatively favorable for the assumption of zonal uniformity, with ice retreat features representative of much of the remainder of the Antarctic ice zone. The sector includes the area off Syowa Station, where  $C$ – $T$  plots of Fig. 3c are shown.

The model was solved numerically with a grid spacing of  $0.25^\circ$  ( $\approx 28 \text{ km}$ ) over a meridional extent of  $\sim 1800 \text{ km}$ , corresponding to the latitude range  $50^\circ$ – $66.25^\circ\text{S}$ . The time step is 10 min and the advection term is calculated at every 10 time steps. No-flux conditions for both  $C$  and  $T$  are applied to the southern and northern boundaries.

To obtain the net flux,  $F_n(x, t)$ , heat flux calculations were made based on the bulk and empirical formulas used in Nihashi and Ohshima (2001a). The calculation includes the surface radiative and turbulent heat fluxes. For atmospheric forcing, ERA-15 data are used. The cloud cover data are obtained from the International Satellite Cloud Climatology Project D2 data. The original grid of the ERA-15 is a Gaussian (N80) grid with an approximate resolution of  $1.125^\circ$ . Figure 5a shows the net heat flux at the water surface from October to February averaged over 1986–93 (climatology).

The wind-forced drift of sea ice is calculated from the geostrophic wind based on ERA-15 sea level pressure, where the sea ice drift is assumed to be 1% of the wind

speed and directed  $18^\circ$  to the left. These choices are based on summer observations in the Arctic with buoys (Thorndike and Colony 1982) because we are focusing on less packed summer ice conditions. Buoy observations in the Weddell Sea showed consistent results for the wind factor (Vihma et al. 1996; Kottmeier and Sellmann 1996). The meridional component of ice drift,  $U(x, t)$ , is averaged over  $25^\circ$ – $45^\circ\text{E}$  for each latitude. Figure 5b shows the meridional component of the wind-forced drift of sea ice from October to February averaged over 1986–93 (climatology). Eastward wind is prevailing around the Antarctic with its speed increasing toward the north up to  $\sim 50^\circ\text{S}$ , and thus sea ice is generally advected northward with a divergent character. While, in the vicinity of the coast of Antarctica, the prevailing wind direction is generally westward, and thus sea ice is advected onshore, resulting in a convergent ice field. This is an area of active ridging and rafting (Martinson and Wamser 1990). The mean ocean currents are zonal in this sector and thus oceanic-forced drift of ice is not included in the model.

The 10-day running means of the net heat flux and wind-forced drift are used for the simulation because we focus on the seasonal time scale and the effects of synoptic disturbances are assumed to be included in the diffusion term. Further, the data from the ERA-15 grid are interpolated onto the model grid.

For initial conditions and comparison, we use ice concentration data obtained from the Special Sensor Microwave Imager (SSM/I) with a resolution of  $\sim 25 \text{ km}$ . For calculation of ice concentration we use the bootstrap algorithm of Comiso (1995), which is considered to be better for the Antarctic Ocean (Comiso et al. 1997). Even if the NASA Team (Cavalieri et al. 1984) and/or enhanced NASA Team (NT2; Markus and Cavalieri 2000) algorithms are used, the results in the following are almost the same. Figure 5c shows the SSM/I ice concentration from October to February in the meridional sector of  $25^\circ$ – $45^\circ\text{E}$  averaged over 1988–2002 (climatology).

We start the calculation from the first of October, when the net heat flux at the water surface shifts to the positive direction at lower latitudes. For the period when the net heat flux is still negative,  $F_n(x, t)$  and  $U(x, t)$  are set to zero. Ice concentration is initialized at the first of October. Initial  $T$  is set to the freezing temperature  $T_f$  ( $= -1.86^\circ\text{C}$ ).

Based on these conditions, we performed a series of model experiments whose description and performance are listed in Table 1. First we present the results for the case in which any dynamical effects are not included under the climatological forcing (local run). In this case the ice concentration is only determined by the local thermodynamical balance [first term of the right-hand side of (4)]. The simulated ice retreat is presented in Fig. 5d. For lower latitudes, positive heat input to the open water from the atmosphere occurs earlier; hence sea ice retreats earlier. Even without dynamical effects,

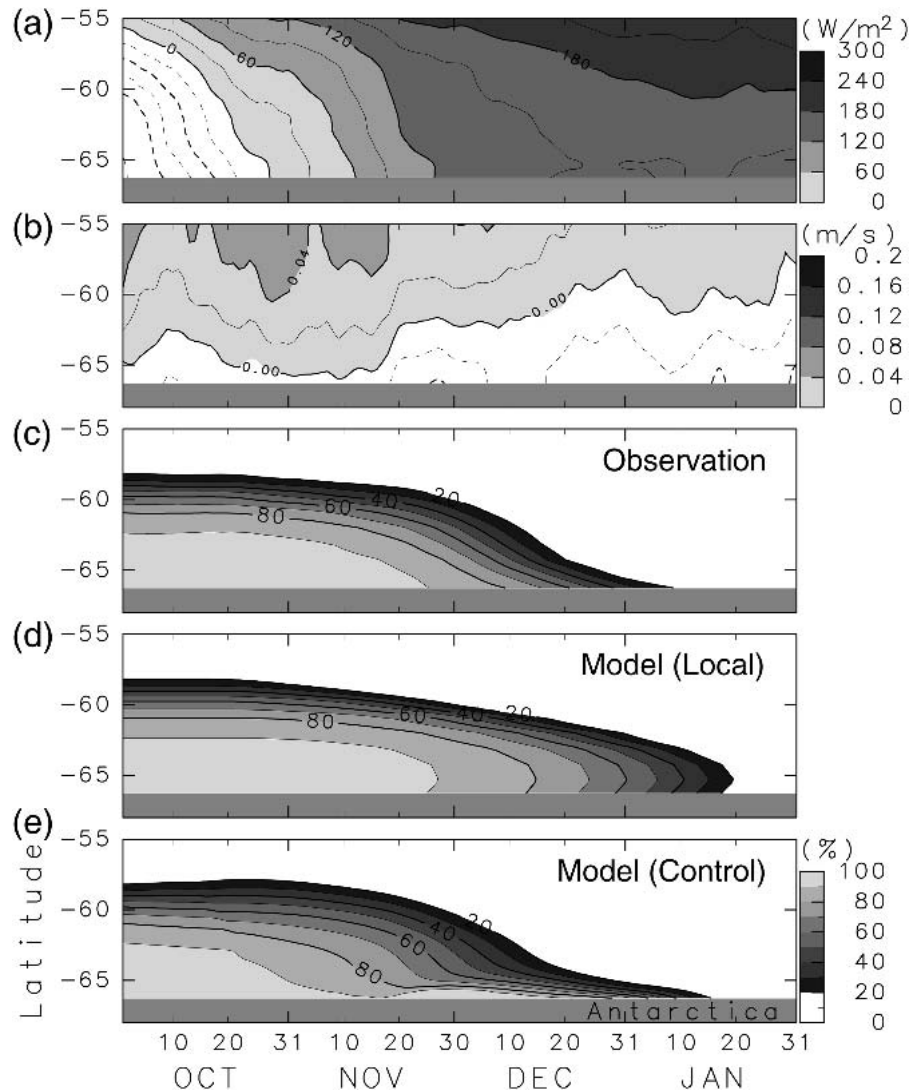


FIG. 5. Atmospheric forcing and ice concentration from observation and models in a meridional sector between  $25^{\circ}$  and  $45^{\circ}$ E from Oct to Jan for the case of climatology. (a) Net heat budget over open water averaged over 1986–93, with the 10-day running means. Positive values (shaded areas) indicate that the ocean gains heat from the air. (b) Meridional component of the wind-forced ice drift averaged over 1986–93, with the 10-day running means, calculated from the ERA-15 geostrophic wind. Positive values (shaded areas) indicate northward drift. (c) Sea ice concentration from the SSM/I observations averaged over 1988–2002. (d) Sea ice concentration, simulated in the local-balanced model under the condition of climatological heat flux (local run). (e) Sea ice concentration, simulated in the two-dimensional model in which the dynamical effects are included under the climatological conditions (control run).

the model roughly reproduces the retreat of sea ice, suggesting that the sea ice retreat is determined by the local balance to a first approximation. When we look at the results in more detail, sea ice remains too late in the area around  $62^{\circ}$ – $65^{\circ}$ S. This area corresponds to the ice divergent zone. This inability to reproduce the observed ice edge is considered to arise mainly from the lack of advection, as will be shown.

Next we present the results for the case that all dynamical effects are included under the climatological

forcing (control run). The simulated ice retreat is presented in Fig. 5e. Reproduction of the sea ice retreat is further improved (see also the model performance in Table 1): sea ice disappears earlier around  $62^{\circ}$ – $65^{\circ}$ S because of the ice divergence effect, when compared with local run.

### c. Open water–albedo feedback

Despite its simplicity, this two-dimensional model can be used to demonstrate the open water (ice)–

TABLE 1. Description and performance of two-dimensional model for  $25^{\circ}$ – $45^{\circ}$ E sector. As an index of model performance, the difference in ice edge (20% ice concentration) location from the observations is used. The bias from the observations, averaged over the period of Nov–Jan (92 days), is presented with the standard deviation. Positive values (degrees of latitude) mean that the model's ice edge is located at a lower latitude. All of the experiments except E5 are from the model with constant ice thickness. Experiment E5 is derived from the model with ice thickness variation.

Expt	Heat flux	Ice drift	Performance
Local	Climatology	No	$1.3^{\circ} \pm 1.4^{\circ}$
Control	Climatology	Climatology	$0.1^{\circ} \pm 0.4^{\circ}$
E1	Climatology	$+2 \text{ cm s}^{-1}$	—
E2	Climatology	$-2 \text{ cm s}^{-1}$	—
E3	1992/93	1992/93	$-0.1^{\circ} \pm 0.6^{\circ}$
E4	1989/90	1989/90	$1.6^{\circ} \pm 0.8^{\circ}$
E5	Climatology	Climatology	$0.9^{\circ} \pm 0.4^{\circ}$

albedo feedback effect. Figure 6 shows the results of two experiments: one is a case in which a northward wind-forced drift anomaly of  $2 \text{ cm s}^{-1}$  is added to the climatological value over the whole period (experiment E1) and in the other a southward wind-forced drift anomaly of  $2 \text{ cm s}^{-1}$  is added (experiment E2), where all other conditions are the same as those of the control run. In the case of E1, because of the stronger northward drift, the ice edge extends northward more rapidly, and the ice concentration in the interior is reduced. As a result, the heat input to the upper ocean is enhanced and the ice melt is accelerated, leading to further decrease in ice concentration. Most of the ice was melted by the middle of December. This feedback can be considered as the open water–albedo feedback since the difference of albedo between ice and open water causes the feedback. By contrast, in the case of E2, the

southward wind-forced drift anomalously keeps the ice concentration high to the south of  $64^{\circ}$ S, which suppresses the heat input through open water. The ice remains near the coast even at the end of January. In what follows, we present this feedback mechanism for specific years.

Figures 7 and 8 show the observations and model results during the 1992/93 and 1989/90 summer seasons, respectively. In the beginning of October, the overall features of the observed ice concentration are similar for the 1992/93 and 1989/90 seasons (Figs. 7c and 8c). However, large differences are apparent in December. During 1992, the ice concentration decreases at all latitudes and most of the ice disappears by the end of December. By contrast, in 1989, the ice disappears rapidly to the north of  $63^{\circ}$ S while high concentrations are maintained to the south of  $64^{\circ}$ S. Even in the middle of January 1990, the ice still remains near the coast. The net heat flux shows only small differences between the two time periods (Figs. 7a and 8a). The differences in ice retreat behavior between the two years likely arose from differences in the wind regime. The wind-forced drift shows that in 1992 (Fig. 7b) the northward drift (eastward wind) was anomalously large and the drift was northward even near the coast during the early melt period (October and November). While in the case of 1989 (Fig. 8b), the southward drift was anomalously large. The 1992/93 and 1989/90 seasons were similar to cases of E1 and E2 in Fig. 6, respectively.

Figures 7d and 8d show the simulated results for the 1992/93 (E3) and 1989/90 (E4) seasons, using a specified initial ice distribution,  $F_n(x, t)$ , and  $U(x, t)$ , for each year. The model agrees well with the observations, although the model performance (see Table 1) is rela-

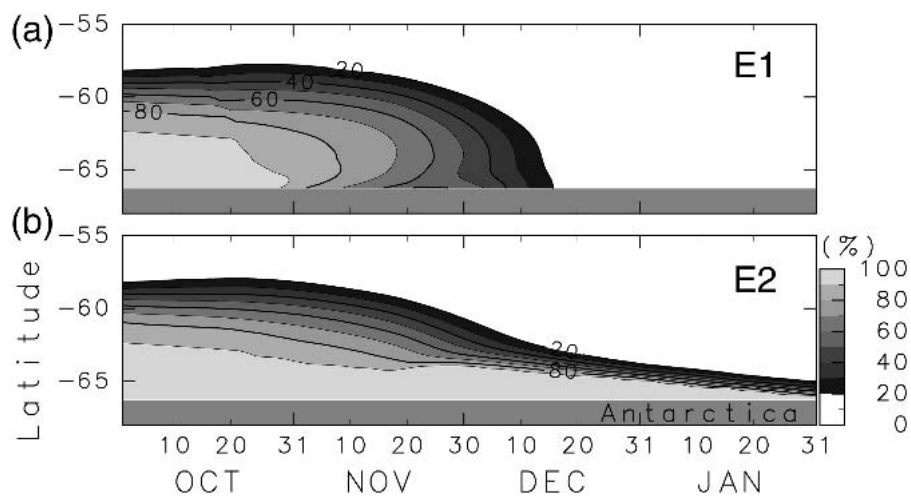


FIG. 6. Time evolution of sea ice concentration (a) for the case that the northward wind-forced drift anomaly of  $2 \text{ cm s}^{-1}$  is added to the climatological value over the whole period (E1) and (b) for the case that the southward wind-forced drift anomaly of  $2 \text{ cm s}^{-1}$  is added (E2), where all other conditions are the same as control run for both cases.

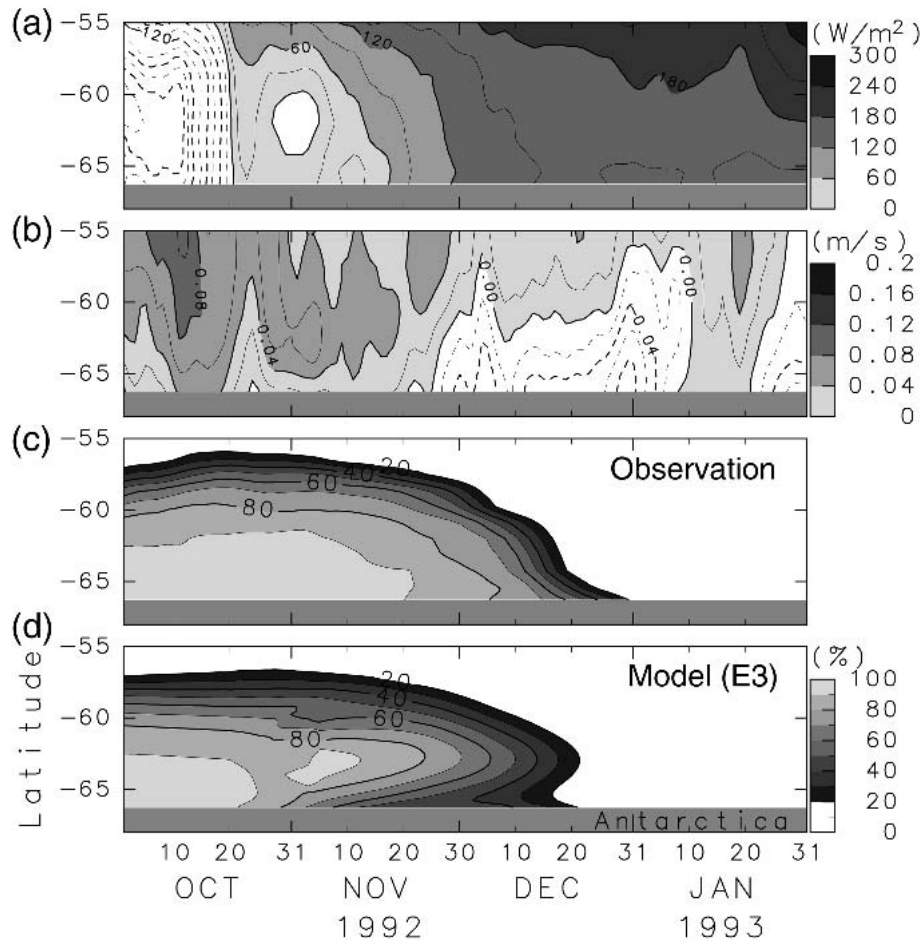


FIG. 7. Atmospheric forcing and ice concentration from observations and model for the 1992/93 season. (a) Net heat budget over open water, with the 10-day running means. (b) Meridional component of the wind-forced ice drift, with the 10-day running means. Positive value (shaded area) indicates the northward drift. (c) Sea ice concentration from the SSM/I observations. (d) Sea ice concentration simulated in the two-dimensional model (E3).

tively low for the 1989/90 season, probably because of insufficient parameterization of ice resistance in the coastal area. In 1992 (Fig. 7d), once the divergent drift decreases the ice concentration, ice melt is accelerated, causing further decrease of ice concentration. By contrast, in 1989 (Fig. 8d), the convergent drift in the coastal area works in the opposite way. The difference between the two experiments is the representation of the open water (ice)–albedo feedback in the ice–ocean coupled system. These results demonstrate that the feedback mechanism can partly explain the year-to-year variation of the sea ice retreat in the Antarctic Ocean.

#### d. Results for the whole Antarctic Ocean

We also performed ice retreat simulations for all sectors ( $10^\circ$  segment longitudinally) around the Antarctic except near the Antarctic Peninsula, under the clima-

tological forcing, in a similar method to section 3b. We used the same parameter values of  $h_0$ ,  $H$ , and  $K_b$  as those of section 3b, with  $F_n(x, t)$  and  $U(x, t)$  given for each sector.

Figure 9 shows the comparison of the monthly mean ice concentration observed by the SSM/I and simulated by the model. The model results are presented as a composite of each sector, calculated independently. Even the local thermodynamic balance model (Fig. 9b) can roughly reproduce the sea ice retreat. When dynamical effects in the meridional direction are included (Fig. 9c), the results are improved. For sectors between  $20^\circ W$  and  $40^\circ E$ , sea ice remains too late in the local balance model (Fig. 9b), while the ice retreats similarly to the observed in the dynamical model (Fig. 9c) because of the positive open water–albedo feedback effect by the divergent ice field. The Ross Sea polynya (around  $180^\circ$ ) is also simulated when including the dynamic effects. However, the model is not able to repro-

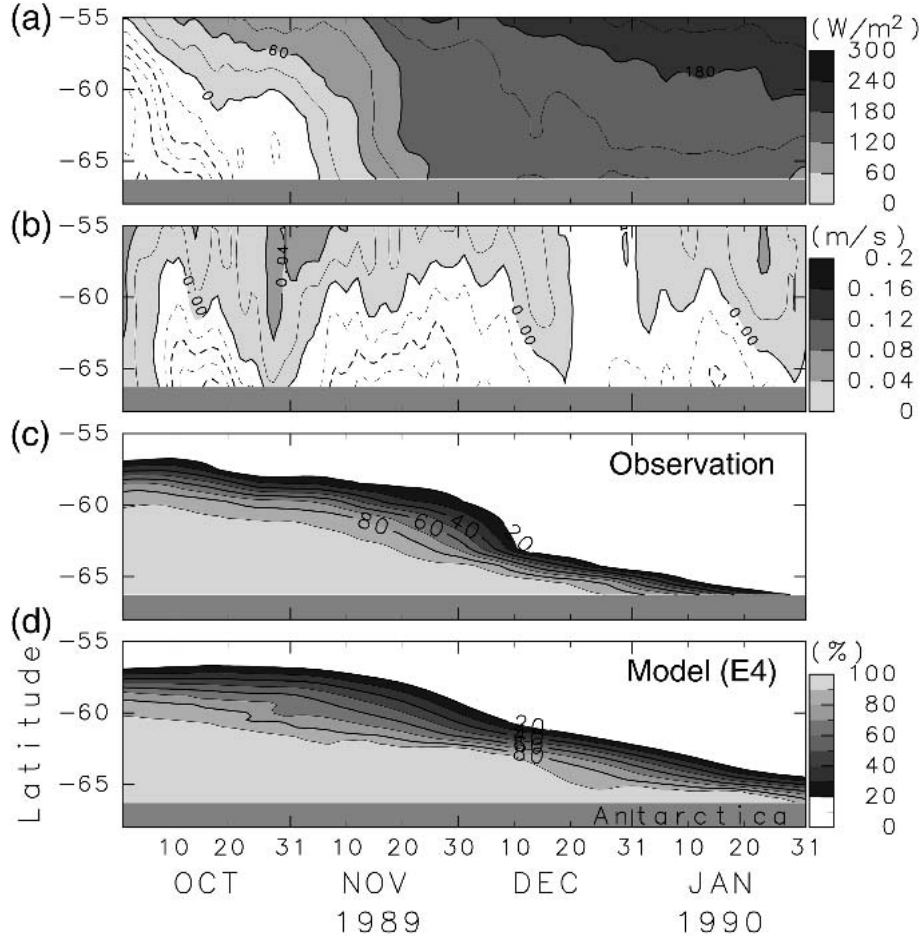


FIG. 8. As in Fig. 7, but for the 1989/90 season.

duce multiyear ice features in the Bellinghausen Sea, Amundsen Sea, and western Weddell Sea, where zonal advection is essential.

**4. A model with ice thickness variation**

Among several simplifications of our model, assumption of constant averaged ice thickness seems too idealistic. Hence we relax this assumption and consider a model that can describe the evolution both of the ice concentration and averaged ice thickness, according to Hibler (1979) or Hibler and Ackley (1983). In their models, in addition to ice concentration  $C(x, t)$ , they defined  $h(x, t)$  as an effective ice thickness averaged over each of the grid cells, including the open water fraction. Thus  $h$  can be regarded as the total ice volume per unit area. Note that the actual averaged thickness is  $h/C$  in this model. Then it is assumed that that sea ice is uniformly distributed between 0 and  $2h/C$  in thickness, and all melts at the same rate. This assumption leads to the following relationship of the local ice melting rate (see Hibler 1979):

$$\frac{dC}{dt} = \frac{dh}{dt} \frac{C}{2h}. \tag{5}$$

As in the previous sections, the melting rate of ice,  $-\rho_i L_f dh/dt$ , is assumed to be  $c_w \rho_w K_b C(T - T_f)$ . Then, with the inclusion of dynamic effects,  $h(x, t)$  is governed by

$$\frac{dh}{dt} = -a_0 C(T - T_f) - U \frac{\partial h}{\partial x} + A_H \frac{\partial^2 h}{\partial x^2} + \psi_h. \tag{6}$$

Using the relationship of (5),  $C(x, t)$  is governed by

$$\frac{dC}{dt} = -\frac{a_0 C^2}{2h} (T - T_f) - U \frac{\partial C}{\partial x} + A_H \frac{\partial^2 C}{\partial x^2} + \psi_C, \tag{7}$$

where  $\psi_C$  is first determined by a similar method to section 3 and then  $\psi_h$  is determined by the same advection correction of  $\psi_C$ .

First we consider the local balance case in which the dynamical terms (second, third, and fourth terms) are dropped in (6) and (7). Then, these two equations along with (3) constitute a system of three nonlinear coupled

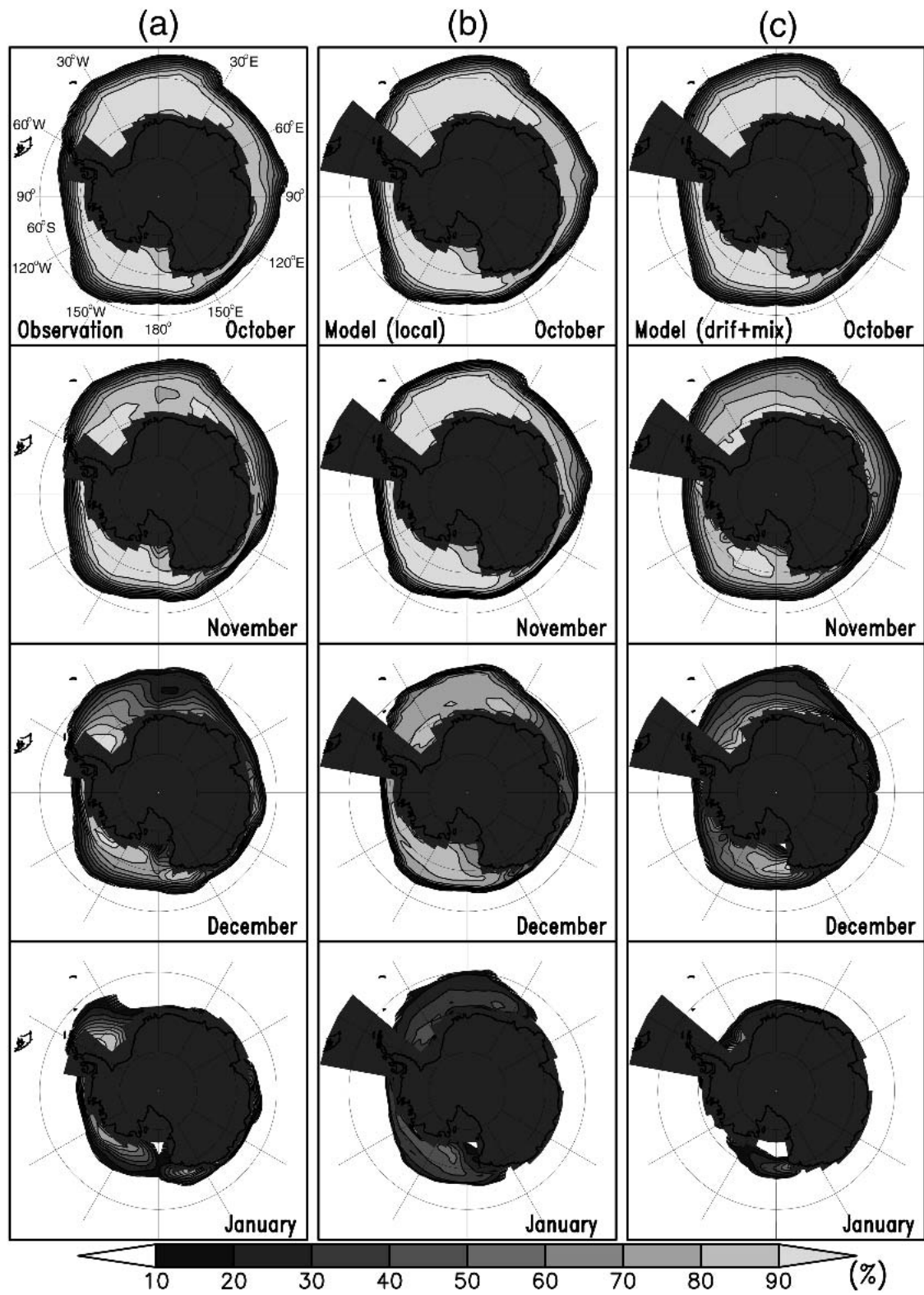


FIG. 9. The monthly mean ice concentration over the whole Antarctic Ocean from (a) the SSM/I observations, (b) results from the local thermodynamical model, and (c) results from the case that the meridional dynamical effects are included.

equations under the constant  $F_n$ . As in section 2, the properties of the solution can be presented in terms of trajectories in the  $(C, T)$  plane (Fig. 10a). Figure 10b shows the ratio of the heat used for ice melt to the heat input through open water, also derived from (3), (6), and (7). Shading curves in Figs. 10a and 10b are the asymptotic curves derived from the model in section 2 with the same parameters. In both figures, the trajectories converge approximately to the same asymptotic curves, except for very low ice concentration in Fig. 10a. This model incorporates the change of ice thickness in a relatively simple way, yet the behavior is similar to the case with a constant ice thickness. The results derived from the models in sections 2 and 4 might be applicable to more sophisticated models and real ocean.

By incorporating all of the dynamical terms (second, third, and fourth terms) in (6) and (7) along with (3), we simulate the meridional ice retreat. Figure 11 is the simulated time evolution of sea ice concentration for

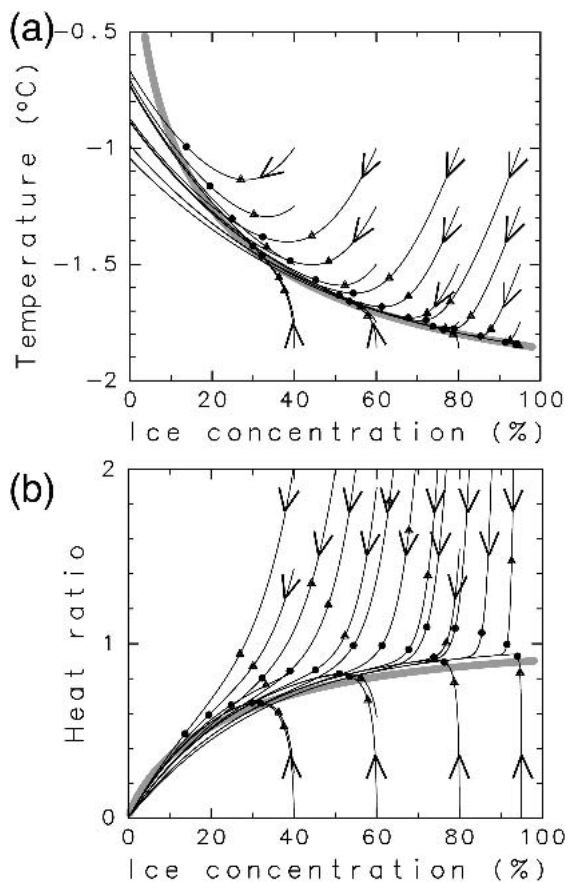


FIG. 10. Time evolution of (a) relationship between ice concentration and upper-ocean temperature and (b) the ratio of the heat used for ice melt to the heat input through open water, derived from the ice–ocean coupled model of (3), (6), and (7). The parameters, initial conditions, and symbols are the same as those of Figs. 3a and 4a. Shading curves are the asymptotic curves derived from the model in section 2 with the same parameters.

25°–45°E sector under the climatological conditions. The sea ice retreat is reproduced to some extent. When compared with the case of the constant averaged thickness (white dotted contour), the ice retreat is somewhat delayed. This is because this model allows the ice melt to reduce ice thickness as well as ice concentration. Using this model, we also performed similar experiments to E1–E4 and similar results were obtained. The open water (ice)–albedo feedback effect can be described also in this model.

## 5. Summary and discussion

In the Antarctic Ocean, sea ice melts mostly by heat input (mainly solar radiation) through open water areas. We propose a simplified ice–upper ocean coupled model in which sea ice melts only by the ocean heat supplied from the air. We treat the ice melt in a bulk way and the melting rate is assumed to be proportional to the difference between the mixed layer temperature and the freezing point multiplied by a bulk heat transfer coefficient ( $K_b$ ).

The model suggests that the ice concentration–mixed layer temperature relationship converges to a specific curve ( $C$ – $T$  relationship) with a time scale of  $H/K_b$  ( $H$ : ocean mixed layer thickness). This well explains the observed concentration–temperature plot ( $C$ – $T$  plot) in the region of 25°–45°E with a spatial averaging of 30 km. The asymptotic (convergent) curve is determined by the two parameters  $F_n/K_b$  and  $h_0/H$  ( $F_n$ : net heat flux,  $h_0$ : averaged ice thickness). In this model  $K_b$  is the key parameter that is hard to be obtained directly by observations, while  $F_n$ ,  $h_0$ , and  $H$  are observable quantities to some extent. Once a  $C$ – $T$  plot can be obtained for a particular area,  $K_b$  can be estimated through fitting to the asymptotic curve. This provides a new useful analysis tool for looking at observational data for sea ice melt and ice–ocean interaction. The plausible value of  $K_b$  is  $1.2 \times 10^{-4} \text{ m s}^{-1}$  from the  $C$ – $T$  plot in the region of 25°–45°E (Fig. 3c). Recently, also in the Ross Sea, the convergent character of concentration–temperature relation was revealed and a similar value of  $K_b$  was suggested (Nihashi et al. 2004).

The model shows that the ratio of the heat used for ice melt to the heat input into open water from the air is inclined to be determined by the ice concentration at that time. If we use this relationship, we may parameterize the melting of sea ice without incorporation of detailed ice–ocean processes in models. Within the range of plausible parameter values and ice concentration in the Antarctic melt season, the ratio ranges mostly between 0.7 and 0.9, suggesting that heat input through open water is mostly used for sea ice melt but not completely.

The model was extended to two dimensions in the meridional direction to simulate ice retreat over the

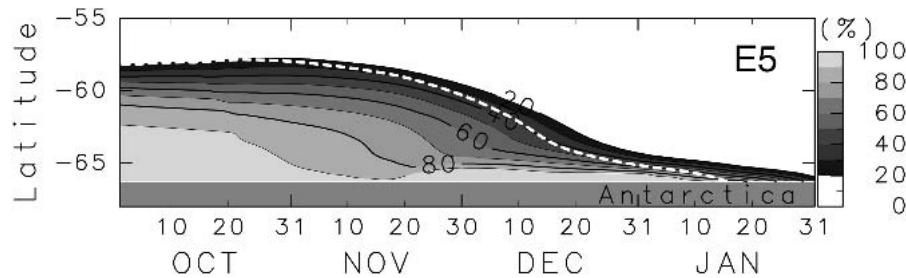


FIG. 11. Time evolution of sea ice concentration in meridional direction simulated in the two-dimensional model of (3), (6), and (7) under the climatological conditions (experiment E5). The ice edge (20% ice concentration) contour derived from the control run (Fig. 5e) is superimposed by white dotted contour.

whole Antarctic Ocean. Even without advection, the ice retreat was roughly reproduced (Figs. 5d and 9b). With the inclusion of dynamic effects in the meridional direction, reproduction of the ice retreat was improved (Figs. 5e and 9c). The ice melt in the divergent region is accelerated by the positive open water–albedo feedback. Nihashi and Ohshima (2001a) showed, through the heat budget analysis in summer, that the total heat input through open water areas from the atmosphere is comparable to the latent heat of sea ice melt in the whole Antarctic sea ice zone. Further, this study suggested that the heat through open water is mostly used for ice melt with a time scale of several days to 10 days. These facts explain that the ice retreat can be roughly reproduced even in the present simple model.

In the ice retreat simulations, we used the value of  $K_b = 1.2 \times 10^{-4} \text{ m s}^{-1}$ , estimated from the  $C-T$  relationship. This choice gave reasonable agreement with the observed ice retreat. The two independent aspects suggested a similar value of  $K_b$ . The value of  $1.2 \times 10^{-4}$  may be a representative value for the Antarctic melt season;  $K_b$  used in our study corresponds to  $c_h \times u_\tau$  ( $c_h$ : heat transfer coefficient;  $u_\tau$ : friction velocity) in some other studies. For the obtained  $K_b$  value of  $1.2 \times 10^{-4} \text{ m s}^{-1}$  and a typical friction velocity ( $u_\tau$ ) of  $0.01 \text{ m s}^{-1}$ ,  $c_h$  comes to  $1.2 \times 10^{-2}$ . This value is the same as that used in the coupled model of Timmermann et al. (2002), but is about 2 times those estimated from direct measurements at the bottom of sea ice (McPhee 1992; MCPhee and Martinson 1994). This difference probably comes from the fact that the heat transfer coefficient in our model is a bulk coefficient that includes lateral melt and melting through brash ice in addition to bottom melt. If the sum of lateral melt and melting through brash ice is the same magnitude as the bottom melt, our value of  $K_b$  is consistent with previous observational results.

Our two-dimensional model demonstrated the following open water (ice)–albedo feedback effect: once the ice concentration is reduced by the divergent wind field, the heat input to the upper ocean is enhanced, leading to further decrease in ice concentration. For a convergent wind field, the ice remains later in the op-

posite sense. This mechanism can partly explain the year-to-year variation of the sea ice retreat in the Antarctic Ocean (Figs. 7 and 8). It should be noted that this feedback accelerates the sea ice anomaly during the active melting season. This may explain the fact that the active ice melt month (December) shows the largest year-to-year variability in ice concentration [Nihashi and Ohshima 2001b; also see the monthly anomaly maps of sea ice in Gloersen et al. (1992)]. Our two-dimensional model can also roughly describe the 1997/98 Ronne polynya (Ackley et al. 2001; Hunke and Ackley 2001) despite the simplicity of the model (results are not shown here). We think that some of the year-to-year variations in summer sea ice in other areas and years can be also explained by open water (ice)–albedo feedback, presented in our two-dimensional model.

We have mostly presented results from the model assuming that the averaged ice thickness is unchanged. This assumption might be an oversimplification. Thus we also used an additional model in which the change of ice thickness is incorporated in a simple way. Similar results were obtained both for  $C-T$  relationship and sea ice retreat simulation (Figs. 10 and 11). Our approach is to model the ice melt as simply as possible and thus we did not use a sophisticated ice–ocean coupled model having the details. In conclusion, to model the Antarctic sea ice melt, inclusion of ice melt process by heat input through open water area is most important, and even the simplified model neglecting other effects can describe the fundamental features of the ice melt. Our simplified approach may be useful for a climate or other model when ones intend to avoid the model complexity or to save the computational expenses.

*Acknowledgments.* The SSM/I data were provided by the National Snow and Ice Data Center (NSIDC), University of Colorado. The manuscript was written when KO was a visiting scholar at School of Oceanography, University of Washington. Critical reading by David Bailey, Steve Ackley, and anonymous reviewers was very helpful for improvement of the manuscript. Most of figures were produced by GFD DENNOU Library. Author KO was supported by Grant-in-Aid for Scien-

tific Research (12640414) and RR2002 of Project for Sustainable Coexistence of Human, Nature and the Earth of the MEXT of the Japanese Government; SN was funded by the National Research Council through a Research Associateship Award at NASA GSFC.

## REFERENCES

- Ackley, S. F., C. A. Geiger, J. C. King, E. C. Hunke, and J. Comiso, 2001: The Ronne polynya of 1997–1998: Observations of air–ice–ocean interaction. *Ann. Glaciol.*, **33**, 425–429.
- Andreas, E. L., and S. F. Ackley, 1982: On the differences in ablation seasons of Arctic and Antarctic sea ice. *J. Atmos. Sci.*, **39**, 440–447.
- Bailey, D. A., and A. H. Lynch, 2000: Development of an Antarctic regional climate system model. Part I: Sea ice and large-scale circulation. *J. Climate*, **13**, 1337–1350.
- Cavalieri, D. J., P. Gloersen, and W. J. Campbell, 1984: Determination of sea ice parameters with the Nimbus 7 SMMR. *J. Geophys. Res.*, **89**, 5355–5369.
- Comiso, J. C., 1995: SSM/I ice concentrations using the Bootstrap algorithm. NASA Ref. Publication 1380, 40 pp.
- , D. J. Cavalieri, C. L. Parkinson, and P. Gloersen, 1997: Passive microwave algorithms for sea ice concentration: A comparison of two techniques. *Remote Sens. Environ.*, **60**, 357–384.
- Drinkwater, M. R., and X. Liu, 2000: Seasonal to interannual variability in Antarctic sea-ice surface melt. *IEEE Trans. Geosci. Remote Sens.*, **38**, 1827–1842.
- Fichefet, T., and M. A. M. Maqueda, 1997: Sensitivity of a global sea ice model to the treatment of ice thermodynamics and dynamics. *J. Geophys. Res.*, **102**, 12 609–12 646.
- , B. Tartinville, and H. Goosse, 2003: Antarctic sea ice variability during 1958–1999: A simulation with a global ice–ocean model. *J. Geophys. Res.*, **108**, 3102, doi:10.1029/2001JC001148.
- Gloersen, P., W. J. Campbell, D. J. Cavalieri, J. C. Comiso, C. L. Parkinson, and J. Zwally, 1992: Arctic and Antarctic sea ice, 1978–1987: Satellite passive microwave observations and analysis. SP-511, NASA, 290 pp.
- Gordon, A. L., and B. A. Huber, 1990: Southern Ocean winter mixed layer. *J. Geophys. Res.*, **95**, 11 655–11 672.
- Häkkinen, S., 1995: Seasonal simulation of the Southern Ocean coupled ice–ocean system. *J. Geophys. Res.*, **100**, 22 733–22 748.
- Hibler, W. D., III, 1979: A dynamic thermodynamic sea–ice model. *J. Phys. Oceanogr.*, **9**, 815–846.
- , and S. F. Ackley, 1983: Numerical simulation of the Weddell Sea pack ice. *J. Geophys. Res.*, **88**, 2873–2887.
- Hunke, E. C., and S. F. Ackley, 2001: A numerical investigation of the 1997–1998 Ronne polynya. *J. Geophys. Res.*, **106**, 22 373–22 382.
- Jeffries, M. O., R. A. Shaw, K. Morris, A. L. Veazey, and H. R. Krouse, 1994: Crystal structure, stable isotopes ( $\delta^{18}\text{O}$ ) and development of sea ice in the Ross, Amundsen, and Bellinghousen Seas, Antarctica. *J. Geophys. Res.*, **99**, 985–995.
- Kottmeier, C., and L. Sellmann, 1996: Atmospheric and oceanic forcing of Weddell Sea ice motion. *J. Geophys. Res.*, **101**, 20 809–20 824.
- Markus, T., and D. J. Cavalieri, 2000: An enhancement of the NASA Team sea ice algorithm. *IEEE Trans. Geosci. Remote Sens.*, **38**, 1387–1398.
- Martinson, D. G., and C. Wamser, 1990: Ice drift and momentum exchange in winter Antarctic pack ice. *J. Geophys. Res.*, **95**, 1741–1755.
- Maykut, G. A., 1986: The surface heat and mass budget. *The Geophysics of Sea Ice*, N. Untersteiner, Ed., Plenum, 395–463.
- , and D. K. Perovich, 1987: The role of shortwave radiation in the summer decay of a sea ice cover. *J. Geophys. Res.*, **92**, 7032–7044.
- McPhee, M. G., 1992: Turbulent heat flux in the upper ocean under sea ice. *J. Geophys. Res.*, **97**, 5365–5379.
- , and D. G. Martinson, 1994: Turbulent mixing under drifting pack ice in the Weddell Sea. *Science*, **263**, 218–221.
- Nihashi, S., and K. I. Ohshima, 2001a: Relationship between the sea ice decay and solar heating through open water in the Antarctic sea ice zone. *J. Geophys. Res.*, **106**, 16 767–16 782.
- , and —, 2001b: Relationship between the sea ice cover in the retreat and advance seasons in the Antarctic Ocean. *Geophys. Res. Lett.*, **28**, 3677–3680.
- , —, M. O. Jeffries, and T. Kawamura, 2004: Melting processes of sea-ice inferred from ice–upper ocean relationship in the Ross Sea, Antarctica. *J. Geophys. Res.*, in press.
- Ogura, T., A. Abe-Ouchi, and H. Hasumi, 2004: Effect of sea ice dynamics on the Antarctic sea ice distribution in a coupled ocean atmosphere model. *J. Geophys. Res.*, **109**, C04025, doi:10.1029/2003JC002022.
- Ohshima, K. I., K. Yoshida, H. Shimoda, M. Wakatsuchi, T. Endoh, and M. Fukuchi, 1998: Relationship between the upper ocean and sea ice during the Antarctic melting season. *J. Geophys. Res.*, **103**, 7601–7615.
- Parkinson, C. L., and W. M. Washington, 1979: A large-scale numerical model of sea ice. *J. Geophys. Res.*, **84**, 311–337.
- Pease, C. H., 1975: A model for the seasonal ablation and accretion of Antarctic sea ice. *AIDJEX Bull.*, **29**, 151–172.
- Roed, L. P., 1984: A thermodynamic coupled ice–ocean model of the marginal ice zone. *J. Phys. Oceanogr.*, **14**, 1921–1929.
- Steele, M., 1992: Sea ice melting and floe geometry in a simple ice–ocean model. *J. Geophys. Res.*, **97**, 17 729–17 738.
- Stössel, A., P. Lemke, and W. B. Owens, 1990: Coupled sea ice–mixed layer simulations for the Southern Ocean. *J. Geophys. Res.*, **95**, 9539–9555.
- , S. J. Kim, and S. S. Drijfhout, 1998: The impact of Southern Ocean sea ice in a global ocean model. *J. Phys. Oceanogr.*, **28**, 1999–2018.
- Thorndike, A. S., and R. Colony, 1982: Sea ice motion in response to geostrophic winds. *J. Geophys. Res.*, **87**, 5845–5852.
- Timmermann, R., H. H. Hellmer, and A. Beckmann, 2002: Simulations of ice–ocean dynamics in the Weddell Sea 1. Model configuration and validation. *J. Geophys. Res.*, **107**, 3024, doi:10.1029/2000JC000741.
- Vihma, T., J. Launiainen, and J. Uotila, 1996: Weddell sea ice drift: Kinematics and wind forcing. *J. Geophys. Res.*, **101**, 18 278–18 296.
- Worby, A. P., R. A. Massom, I. Allison, V. I. Lytle, and P. Heil, 1998: East Antarctic sea ice: A review of its structure, properties and drift. *Antarctic Sea Ice: Physical Processes, Interactions and Variability*, M. O. Jeffries, Ed., Antarctic Research Series, No. 74, Amer. Geophys. Union, 41–67.
- Wu, X., I. Simmonds, and W. F. Budd, 1997: Modeling of Antarctic sea ice in a general circulation model. *J. Climate*, **10**, 593–609.